THE PENNSYLVANIA STATE UNIVERSITY
SCHREYER HONORS COLLEGE

JOHN AND WILLIE LEONE FAMILY DEPARTMENT OF ENERGY AND MINERAL ENGINEERING

# IRRADIANCE MODELING VARIANCE ON VERTICAL PLANE OF ARRAY SURFACES

SCOTT BURGER
SPRING 2013

A thesis
submitted in partial fulfillment
of the requirements
for a baccalaureate degree
in Energy Engineering
with honors in Energy Engineering

Reviewed and approved* by the following:

Jeffrey R.S. Brownson
Associate Professor of Energy and Mineral Engineering
Thesis Advisor

Sarma Pisupati
Associate Professor of Energy and Mineral Engineering
Honors Adviser

*Signatures are on file in the Schreyer Honors College.

# Abstract

Significant radiative transfer occurs outside of buildings, yet energy control systems are typically signaled by internal air temperature thermostats. As façades essentially behave as flat plate solar thermal collectors, windows permit rooms to behave as cavity collectors. It is believed that buildings may perform at higher economic efficiency with external signals. An analysis of measured irradiance for plane of array (POA) vertical surfaces was compared to modeled irradiance data (TRNSYS) to evaluate residuals. The measured POA irradiance data integrates all irradiance components for a given orientation, collected on minute intervals for half of the year between the months of July and December. The data were available for the East, West, and North surfaces of the Energy Efficient Buildings Hub's Building 101 in the Philadelphia Navy Yard. Modeled data was generated from global horizontal irradiance from a meteorological station in Avondale, Pennsylvania, located thirty three miles from the Philadelphia Navy Yard. Comparative analyses between irradiance data averaged over each hour and irradiance collected from Avondale, PA resulted in occasional residuals on the order of hundreds of watts per meter squared. To evaluate if the residuals between the measured and modeled data were considered statistically different, a $t$-test was employed to compare each B101 sensors' average irradiances with Avondale's average irradiances for each month from July to December. The results of the $t$-tests proved with 95% confidence that between the months of August and December for the North and East walls and during the month of July for the West wall, the measured irradiance values were statistically different from the modeled irradiance values due mostly to surrounding objects. As a result, the modeled data cannot represent the measured data during those months. Use of local sensors that report actual shading conditions upon a building are actually more useful in this case, as a shaded region will lead to reduced energy gains for entire zones of the building, and require control response to maintain a comfortable indoor environment. Solar irradiance varies significantly on a building's many surfaces based on the environment and surrounding objects. This case study shows how local *plane of array* irradiance data can be informative to a building control system.

# Table of Contents

# List of Figures

# Acknowledgments

First, I would like to express my great appreciation to Dr. Jeffrey Brownson for his influential passion in all aspects of solar energy and for his acceptance of me into the Brownson Research Group as an undergraduate student. I also want to thank Dr. Brownson for his valuable collaboration and guidance throughout the planning, development, and revision of this research work. Second, and most importantly, my sincerest thanks to Lucas Witmer, who helped me plan, develop, organize, and guide the completion of this work. His daily assistance and knowledge was instrumental in my development as an engineer and scientist. Third, I would like to express my gratitude for the motivation and support from the entire Brownson Research Group. Finally, I would like to thank my loving family for their continued support throughout my entire educational career and their emphasis on the importance of always trying my best.

Chapter 1

# Introduction

## 1.1 Background

Significant radiative transfer occurs outside of buildings, yet energy control systems are typically signaled by internal air temperature thermostats. These reactionary energy control systems inefficiently handle heating and cooling loads in residential and commercial sectors. In 2011, approximately 41% of total energy consumption in the United States was from residential and commercial buildings.[4] In 2003, commercial buildings (i.e. education facilities, health care facilities, and office buildings) consumed 659 trillion BTUs (∼18%) of electricity which provided energy for space heating and cooling.[4]

To reduce heating and cooling energy consumption, buildings utilize passive systems to absorb, admit, emit, and reflect solar insolation (irradiance incident on a surface).[5] Overhangs or shading devices and insulation are examples of passive systems to reduce building energy consumption.[5] Building façades essentially behave as flat plate solar thermal collectors (absorbs/stores irradiance), while windows permit rooms to behave as cavity collectors (admits and stores irradiance). Based on the thermal properties of a building, heating and cooling loads increase to compensate for the storage of heat.

There is potential for buildings to perform at higher economic efficiencies with external signals. Accurate Plane of Array (POA) irradiance measurements collected by sensors are valuable in the solar resource evaluation of a given site. Sometimes it can be advantageous to mount sensors along the plane of array (at an angle or vertically). For example, sensors are mounted on the same plane as photovoltaic arrays to simulate the amount of energy that would be incident on those arrays. Vertical POA sensors are beneficial for measuring irradiance on vertical surfaces such as building walls and façades. Vertical POA irradiance on building walls can play a role in heat transfer in a building. The belief is that the information a set of vertical POA sensors

provides is useful for efficient building controls responding to changes in the outside environment.

### 1.1.1 Energy Efficient Buildings Hub

Established by the United States Department of Energy (DOE) in the Philadelphia Navy Yard in Philadelphia, Pennsylvania in 2011, the Energy Efficient Buildings Hub (EEB Hub) is lead by the Pennsylvania State University. The EEB Hub is composed of 22 organizations including research universities, DOE laboratories, industrial firms, economic development agencies, and community and technical colleges.[6] The Hub seeks to develop energy efficient retrofits to existing buildings in the Navy Yard as well as in the Greater Philadelphia region. It is a catalyst for improving building energy efficiency with the goal of reducing commercial building energy use by 20% by 2020, and it also promotes economic growth and job creation in the Navy Yard.

Located in the Navy Yard as the headquarters of the EEB Hub, Building 101 (B101) is a highly instrumented commercial building.[7] Figure 1.1 provides a birds-eye view of the Navy Yard and B101. The sensor instruments and data loggers provide data points and measurements of airflow, energy balances, and indoor air quality parameter baselines throughout the interior and exterior of the building. The irradiance data values for the North, East, and West walls are collected by LICOR LI200X silicon pyranometers pictured in Figure 1.2.[8] Based on simulation models of these building systems, the impact of retrofit improvements are quantified. Forward models are coordinated with the National Renewable Energy Laboratory (NREL) who are developing predictive models to estimate the load demand, energy utilization, indoor environment quality, and lighting levels.[7] These predictive models will quantify the impact that building retrofits have on the energy efficiency of a building, and it can be applied to other buildings in the Greater Philadelphia region, as well.


**Figure 1.1.** Picture of (left) the Philadelphia Navy Yard with a box around the location of Building 101 and (right) a birds-eye view of Building 101.


**Figure 1.2.** Installation apparatus for the LI200X pyranometer on the East Wall of B101.

### 1.1.2 National Oceanic and Atmospheric Administration

The National Oceanic and Atmospheric Administration's (NOAA) National Climatic Data Center (NCDC) maintains the world's largest climate data archive. Data ranges include paleoclimatic data all the way to data less than an hour old.[9] Within the NCDC is the United States Climate Reference Network (USCRN) which includes climate data from 221 locations in the United States. Core measurements include air temperature, precipitation, solar radiation, and wind speed. Choosing a USCRN site, especially to measure solar radiation, is based on a number of factors including regional and spatial representation, climate consistency, long term site stability, and proximity to other observing sites. Avondale, Pennsylvania was chosen for its consistent climate and open, unobstructed landscape. In other words, there are no trees or other potential shading objects nearby. Also, the Avondale location is located adjacent to the Stroud Water Center. The USCRN measures solar resource because radiation data is needed to develop

the relationship between local air temperature and air temperature from nearby data collection sites. Solar radiation is also used to assess cloud types for agricultural and hydro-meteorological models.[10]

Component-based irradiance data, such as beam and diffuse radiation, can be collected by a pyrheliometer or a shadowband radiometer, but this data is relatively expensive and not readily available for most locations.[11] Global irradiance data is more widely available and can be used to calculate the irradiation components (beam and diffuse) by various methods such as the Perez Model.[12] Pyranometers are a type of radiometer, which is a device used to measure radiant flux. In the case of a pyranometer, it measures the radiation from the sun. There are two different types of pyranometers: blackbody and silicon-cell. Blackbody pyranometers have a spectral response of 280-2800 nm and cost anywhere between $1000 and $5000 while silicon pyranometers are about 10% of that cost. Since most solar panels use silicon as the primary semiconductor, silicon pyranometers have a similar spectral response (300-1100 nm) as a solar panel. As a result, silicon pyranometers provide a more accurate representation of the energy available for conversion to electricity by a solar panel at a tenth of the cost of a blackbody pyranometer.[13]

The irradiance data was measured in Avondale using a Kipp & Zonen SP Lite silicon pyranometer as shown in Figure 1.3. The SP Lite computes data by obtaining the voltage every two seconds and averaging the voltages every 5 minutes. The twelve 5 minute periods are converted to irradiance ($W/m^2$) by using a linear regression calibration equation and then averaging those values to obtain the global horizontal irradiance (GHI).[1]

**Figure 1.3.** Picture of the Kipp & Zonen pyranometer in Avondale, PA.[1]

## 1.2 Literature Review

### 1.2.1 Types of Irradiance

The data values collected in Avondale and the Navy Yard are labeled as irradiance (units of $W/m^2$) which is the rate at which radiant energy is incident on a surface per unit area of that surface.[12] For the purposes of this study, the Avondale irradiance data is labeled as "modeled" while the Building 101 irradiance data is labeled as "measured". Irradiance values are instantaneous values over a specified area as opposed to being over a specific time period. Total solar irradiance, or more commonly global horizontal irradiance (GHI), is the sum of two components of irradiance: beam irradiance and diffuse irradiance as shown in Equation 1.1.[5] Figure 1.4 shows the components of GHI. Beam irradiance ($G_B$), or direct irradiance, is the solar irradiance received from the sun without having been scattered by the atmosphere. On the other hand, irradiance received from the sun that has its direction changed due to scattering in the atmosphere is known as diffuse irradiance ($G_D$).[12] In contrast to GHI is plane of array (POA) irradiance. POA irradiance is incident on a surface at some angle from horizontal. In the case of Building 101, the sensors are mounted on the vertical plane of array.

$$G = G_B + G_D \tag{1.1}$$

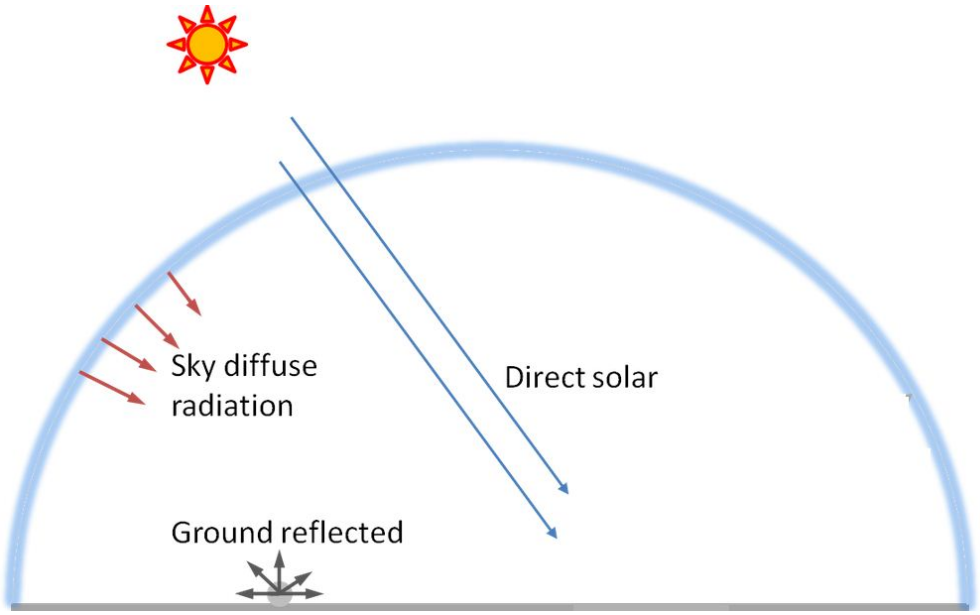


**Figure 1.4.** Sky dome with beam irradiance, diffuse irradiance, and ground-reflected irradiance.[2]

Figure 1.5 shows the relationship between the beam irradiance component normal to a surface and the tilted beam irradiance component. Therefore, the amount of irradiance on a tilted surface is a sum of the beam ($G_B$), diffuse ($G_D$), and ground-reflected irradiance as shown in Equation 1.2[5], where $G_G$ is the ground-reflected irradiance component.

$$G_t = G_{Bt} + G_{Dt} + G_{Gt} \tag{1.2}$$

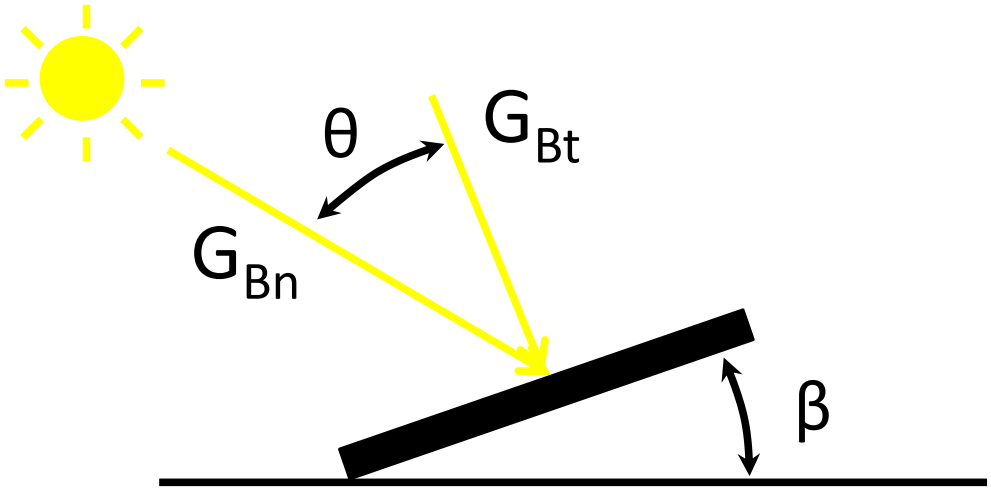


**Figure 1.5.** Relationship between the beam irradiance component normal to a surface and the tilted beam irradiance component.

### 1.2.2 History of Vertical Surface Irradiance Measurements

Due to the increase in solar energy usage to supplement conventional fuel sources, there is an increase in demand for inexpensive, accurate solar resource data for a given location. Realistically, solar panels are often mounted on an inclined surface, such as a roof, to maximize insolation, and the majority of irradiance incident on a building hits the building's vertical façade rather than a horizontal plane. For years, however, irradiance was measured on horizontal surfaces rather than on inclined or vertical surfaces.[14]

In 1986, a study was performed by Maxwell to compare irradiance measured from vertically-mounted pyranometers to global irradiance on tilted surfaces that was converted from GHI at the Solar Radiation Research Laboratory in Golden, CO. Vertical POA irradiance data was collected concurrently with the GHI data 2 years prior over a 169-day period between the months of July and December ending on December 31, 1984. Maxwell looked at isotropic, anisotropic, and a combination of both situations for the diffuse and ground-reflected irradiance for the vertical POA surfaces. Maxwell used five different transposition algorithms to convert the GHI to global irradiance on tilted (vertical) surfaces for north-facing, south-facing, east-facing, and west-facing sensors. Maxwell's results showed that all five transposition models overestimated irradiance by 18%-46.5% on the vertical, north-facing sensors. Four out of the five models predicted the south-facing irradiance within ±5%. Finally, the east and west-facing irradiance values had errors ranging between -3% and 23%. One of Maxwell's transposition models, the Perez Model, which was used as the conversion model in TRNSYS for Avondale, yielded important results. The Perez Model overpredicted the irradiance on the north-facing, south-facing, and west-facing vertical surfaces. The irradiance on the north-, south-, and west-facing surfaces were overpredicted by 18.0%, 6.7%, and 10.6%, respectively. These results showed that there is a significant deficiency in the diffuse sky irradiance component in the Perez Model as well as the other conversion algorithms.[15] A similar study performed by Stoffel in 1987 viewed irradiance values during the same year as Maxwell's study (1984) but only looked at a 41 day period between July 22 and September 4. Again, these results showed a large overestimation of north-facing surfaces but a better approximation for south-facing surfaces.[16] Both studies stressed the need for deeper research into vertical POA irradiance measurements. Both Maxwell and Stoffel believed that more research into vertical POA irradiance would lead to a deeper understanding of the deficiency in predicting diffuse sky irradiance.[15][16]

A similar study by Gueymard in 2009 compared irradiance values collected from south-facing sensors mounted vertically and 40° from horizontal to predictions from ten tranposition models of horizontal irradiance in Golden, CO. When only global horizontal irradiance is known, the accuracy of predicting POA irradiance (in this case, vertical and 40°) significantly degrades due to inaccurate diffuse irradiance predictions. In addition, Gueymard points out that the vertical sensor saw even greater prediction inaccuracies due to errors in the ground-reflected calculations.

Just like Maxwell and Stoffel, Gueymard concluded that further research was needed to more accurately predict POA irradiance from global horizontal irradiance. Also, Gueymard showed that the prediction of irradiance on tilted surfaces is important to the effective, accurate measurement of solar resource for a given site.[11]

### 1.2.3 Challenges of Attaining Accurate Solar Resource Data

The irradiance data collected by NOAA in Avondale is only global horizontal irradiance (GHI), which is labeled by Gueymard as a suboptimal input in assessing the solar resource of a location.[11] As a result, irradiance measured on tilted surfaces is more meaningful to assessing the solar resource of a given location.

Measuring GHI at a site is the most common method to assessing the solar resource. Only one sensor is required which cuts costs compared to purchasing multiple sensors. However, accuracy in irradiance data is sacrificed by only considering GHI rather than incorporating specific direct and diffuse irradiance. Consequently, NOAA's Avondale site provides suboptimal input GHI compared to B101's multi-sensor arrangement. The pyranometers mounted on the East, West, and North walls of B101 measure the total irradiance by including direct and diffuse irradiance. While the specific ground albedo is not known at B101, the irradiance data in the Navy Yard is closer to an optimal input than the GHI data from Avondale. Maxwell, Stoffel, and Gueymard proved that the large deficiency in predicting diffuse irradiance leads to inaccurate predictions of tilted irradiance from GHI data.

To more accurately measure solar resource availability, data is typically measured at timesteps of one minute or less.[11] However, most transposition models such as Hay[14], Perez[17], and Reindl[18] were developed using hourly timesteps of irradiation data. More accurate solar resource availability is necessary for evaluating a potential site, especially a large-scale solar project. Expensive, large-scale solar projects (commercial, utility-scale, etc.) are highly dependent on profitability and may not allow for irradiance calculation tolerances larger than $\pm 5\%$.[11] Large-scale projects require large investments and require more accurate results to ensure long-term profitability.

Due to geographical differences in two different locations, there are challenges with shading effects from cloud cover and nearby buildings as well as reflective surfaces (ground albedo or nearby object albedo). Incorrect calculation or observance of shading regions can lead to gross overestimations or underestimations of irradiance at a given site. Unlike buildings which have regular geometries and, as a result, predictable shading patterns, objects such as trees have irregular geometries and make it difficult to develop shading profiles.[12] As well as irregular shapes, deciduous trees provide different shading profiles based on the time of year, making shading predictions even more difficult. Deciduous trees in the spring and summer provide sig-

nificantly more shading than in the fall and winter due to increased foliage. Local climates and landscapes also influence the measurement of irradiance and affect the solar resource availability. The albedo, or reflectance, of Earth's surface as well as surrounding objects heavily influence the ground-reflected irradiance component. Large albedos (high surface reflectivity) can amplify the irradiance measurements on tilted surfaces, and this phenomenon can lead to significant error in the estimation of irradiance on a plane of array surface.[19] Since the ground albedos of Avondale and Building 101 are not known, the widely accepted value of 0.2 was used. In urban environments, the albedo of surrounding building façades or streets depends on the material such as concrete (0.29) or asphalt (0.08).[20].

In addition to shading from nearby objects, effects from cloud shading create challenges for comparing two different locations. It is difficult to model and predict changes in cloud cover between the Philadelphia Navy Yard and Avondale, PA which is located 33 miles west of the Navy Yard.

Chapter 2

# Methods

## 2.1 Data Processing and TRNSYS

### 2.1.1 Avondale Data Collection and Processing

The remote data source for correlation analysis was collected from the National Oceanic and Atmospheric Administration (NOAA) meteorological station in Avondale, PA, located approximately 33 miles west of the Philadelphia Navy Yard. The data was adjusted for this geographic difference, but short term differences created by scattered clouds or microclimatic difference are not accounted for. Over timesteps of one hour, the impact of these differences is assumed to be small. The GHI was downloaded from the Avondale weather station for use with model correlations as a comma-separated values (CSV) file.[21] Due to the large quantity of irradiance data, each month of the year was downloaded separately rather than as one large data set for the entire year. The CSV file was imported into Microsoft Excel where a macro was run to remove unnecessary data or to use interpolation to fill in missing data points. After the macro was run, the CSV file was imported into TRNSYS using a data reader (Type 9c). The Avondale data was converted to kJ/hr·m$^2$ and run through a radiation processor (Type 16a), where some geographical details and model assumptions were made. The radiation processor uses the Perez model as the tilted surface mode to convert the GHI data to simulate the irradiance hitting a vertical wall. The latitude and solar shift of Avondale with respect to the Navy Yard provided the necessary geographical details. The output from the radiation processor was passed through a unit conversion routine to convert the irradiance data back to W/m$^2$ and finally through a graphical output component.

### 2.1.2 Building 101 Data Collection and Processing

The measured POA (vertical) data from Building 101 must also be downloaded. The irradiance values incident on the East, West, and North walls on minute intervals of Building 101 were

downloaded from the EEB Hub's website.[8] The irradiance data from the EEB Hub sensors are in units of $W/m^2$.

With the data in tabulated files, Microsoft Excel macros were developed to process the data for easy import into TRNSYS. Both data sets were reviewed for gaps and corrected by interpolation, typically occurring during the nights. In addition, the macros also converted the minute data to hourly data by averaging all 60 data points over each hour. After the data sets were corrected and converted to hourly data, the tabulated files were imported into TRNSYS. The TRNSYS model for Building 101 employed a second data reader (Type 9c). The output from the data reader was passed through the same graphical output component as the Avondale data. Figure 2.1 displays the TRNSYS simulation studio layout with the combined functions for Avondale and Building 101.

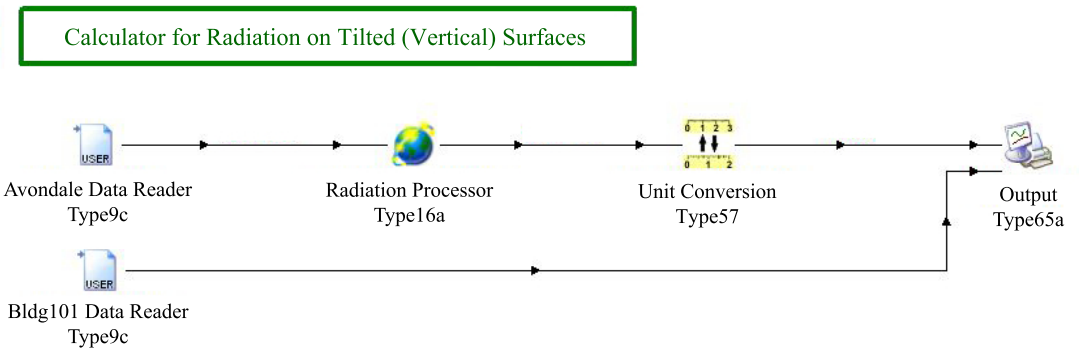


**Figure 2.1.** TRNSYS screen shot of the simulation studio for the Avondale and Building 101 data.

## 2.2 Error Calculation and Graphical Approach

The output from the TRNSYS model yields tabulated measured irradiance data from Building 101 and modeled data from Avondale, where the vertical surface irradiance is estimated by component derivation from Avondale GHI. The differential irradiance and error between the measured and modeled data for each wall was calculated using Equations 2.1 and 2.2, respectively. Using the difference in irradiance, percent error, and global horizontal irradiance for each month, data for each wall was combined into a single tabulated file. From that set, the lower quartile, minimum, median, upper quartile, maximum, and mean at each hour for each wall was evaluated, as well as GHI. Using Equation 2.3, weighted averages were calculated for each wall, where $x$ is the data set and $w$ the weighted value. The weighting criterion was based off the mean horizontal irradiances for each hour in Avondale. Weighting the residuals is important to highlight significant irradiance residuals. In other words, the residuals are emphasized in the middle of the day rather than in the early morning or late evening hours.

$$\text{Residual} = \text{Measured} - \text{Modeled} \tag{2.1}$$

$$\%\text{Residual} = \frac{\text{Measured} - \text{Modeled}}{\text{Modeled}} \tag{2.2}$$

$$\bar{x} = \frac{\sum_{i=1}^{n} x_i w_i}{\sum_{i=1}^{n} w_i} \tag{2.3}$$

With the weighted averages for each wall, the mean irradiance was estimated on each wall and summed. Using Equation 2.3 again, the weighted mean error and the weighted mean percent error was also calculated. Box and whisker plots were generated for each wall to show the error values, or residuals, during each hour of the day for each month analyzed, offering a new perspective on the hourly distributions of error.

The relationship between two variables is typically viewed through the lens of a dependent/ independent combination. The dependent variable is typically called the "criterion" variable while the independent variable is typically called the "regressor" variable. However, the dependent variable does not always imply a cause-and-effect relationship. In cases like this, a relationship between two variables is termed a simple regression.[3] In the case of Avondale and Building 101, Avondale irradiance is referred to as "modeled" data while Building 101 irradiance is referred to as "measured" data. Despite being labeled as "modeled", the irradiance values for Avondale are still subject to various errors and assumptions that lead to imperfect data.

Rather than looking at the error between both sets of data (which assumes that one data set is "perfect" data), the residual provides a greater mode of comparison between both data sets since neither one contains "perfect data". The residual is a departure or difference of an actual $Y_i$ from a predicted $Y_i$. In the case of comparing Avondale and Building 101 irradiance, the modeled data (Avondale) is the predicted $Y_i$ while the measured data (Building 101) is the actual $Y_i$.

To determine whether the difference between two values is significant, a simple $t$-test can be used, commonly referred to as the "Student's" $t$-test. Specifically, a "Student's" $t$-test compares two data sets to see if they are statistically different from one another. A "Student's" $t$-test assumes a normal distribution and determines the difference between a population mean and a hypothesized mean, also known as the null hypothesis.[3] The Welch's $t$-test is an approximation of the "Student's" $t$-test that compares two data sets that possibly have unequal variances, which is the case of the Avondale and Building 101 data sets. The results of the Welch's $t$-test yields a "$t$-statistic" that can be compared with a table of probabilities to show the probability that the difference between a population mean and a hypothesized mean is statistically significant. In other words, the results of Welch's $t$-test shows the probability that the irradiance values for Avondale and Building 101 are statistically different. If the probability is high that both data sets are statistically different, then the null hypothesis is rejected.[22]

To calculate the $t$-statistic in a $t$-test, the variance (VAR) and the standard error of the mean (SEM) need to be calculated as shown in Equations 2.4 and 2.5[3], where $x_i$ is a given irradiance, $\bar{x}$ is the mean irradiance value, and $n$ is the number of data points in the entire set. Using the population mean ($\bar{x}_2$), null hypothesis ($\bar{x}_1$), and SEM, the $t$-statistic can be calculated as shown in Equation 2.7.[3] Comparing this $t$-statistic to the probability table shown in Figure A.1 will yield the confidence interval that the result is statistically significant.

$$VAR = \frac{\sum (x_i - \bar{x})^2}{n} \tag{2.4}$$

$$SEM = \sqrt{\frac{VAR_1^2}{n_1} + \frac{VAR_2^2}{n_2}} \tag{2.5}$$

$$\nu = \frac{\left(\frac{VAR_1^2}{n_1} + \frac{VAR_2^2}{n_2}\right)^2}{\frac{\left(\frac{VAR_1^2}{n_1}\right)^2}{n_1 - 1} + \frac{\left(\frac{VAR_2^2}{n_2}\right)^2}{n_2 - 1}} \tag{2.6}$$

$$t = \frac{\bar{x}_1 - \bar{x}_2}{SEM} \tag{2.7}$$

Chapter 3

# Results and Discussion

Figure 3.1 demonstrates the daily residual errors between the modeled values and the measured POA data. The top line of daily GHI is the source data from Avondale during a select clear sky week. The residual differences between measured and modeled vertical surface irradiance for the East, West, and North façades are represented below that primary GHI set. Repetitive errors of a sinusoidal over/under prediction can be observed each morning in the East, each afternoon for the West, and for both periods to the North.

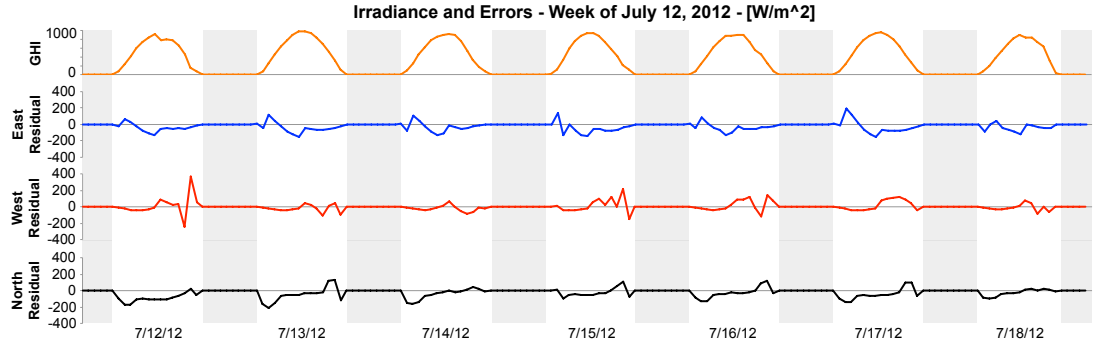


**Figure 3.1.** Building 101 errors assess for GHI and POA during the week of July 12-July 18, 2012

From detailed single-day inspections, the modeled vertical surface irradiation for Avondale was found to be similar yet not equivalent to the measured Building 101 data. Figure 3.2 shows a day's comparison between measured POA data and modeled data from Avondale, using the example of a sunny day in July. Figure 3.3 displays an example of an alternate cloudy day in July.

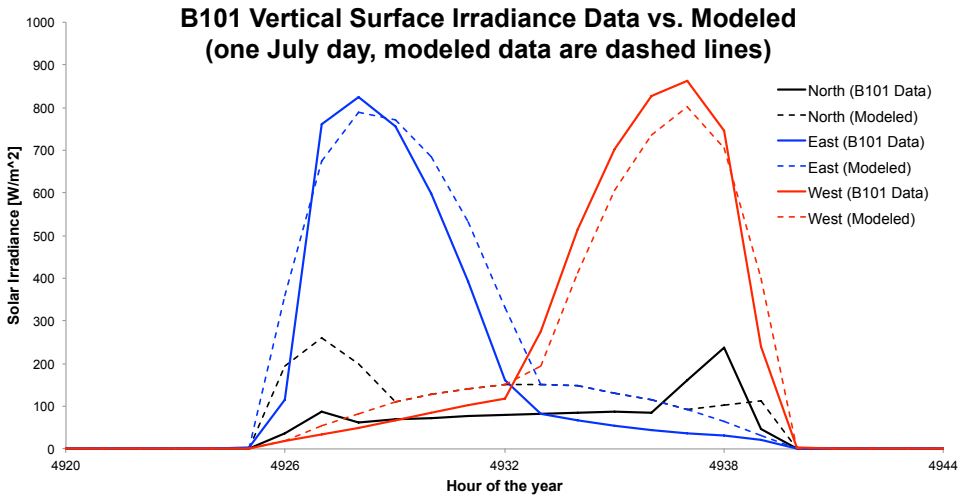


**Figure 3.2.** A sunny day on July 6, modeled data is dashed, measured data is solid.

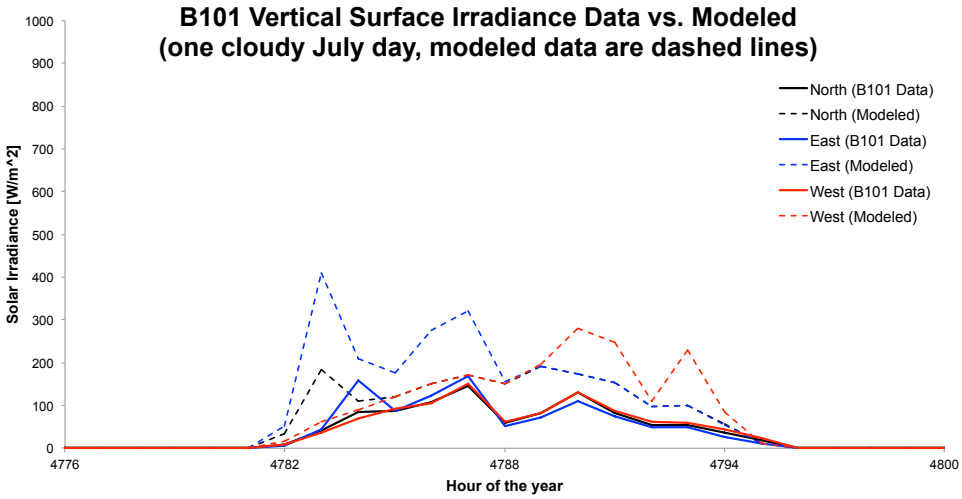


**Figure 3.3.** A cloudy day on July 20, modeled data is dashed, measured data is solid.

Figure 3.4 shows the transition time in October where the East sensor starts in full sun all morning and ends the month shaded by a building wing during most of the morning. Hence, the East sensor is completely shaded for the month of December and half of January, but is not shaded by the building wing-wall from the beginning of March through early October. Phenomena such as this were delivered strong biases and skewing of the error data analyses for different months and times of the day.

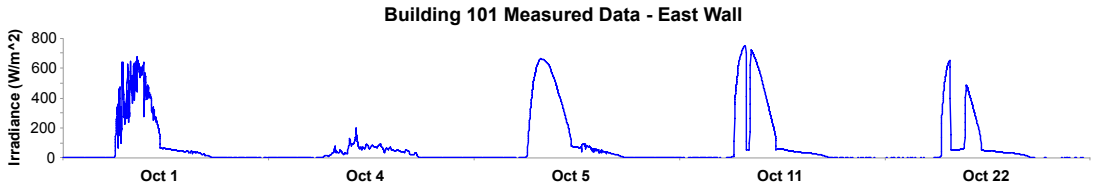


**Figure 3.4.** Building 101 East sensor data for select clear days during the month of October, showing a transition from fully exposed to partially shaded.

Figures 3.5, 3.6, and 3.7 provide a detailed and highly informative perspective on the evolution of hourly residuals among each of the three Building 101 vertical surfaces. The box and whisker plots show the hourly spread of data for each month analyzed, from July 2012 through December 2012. In certain cases the maximum observed point was outside the bounds of the standardized plots–the values were then labeled on the graphs.

Figure 3.5 shows residuals from the East sensor that increase in the morning in both magnitude and skew as time progresses from July to December. This is due to the significant shading that obscures the East sensor during the 10am hour in October and most of the day in both November and December. The East sensor is located in a transition shade region by building wingwall interference located Southeast of the pyranometer as shown in Figure 3.8. The positive residuals earlier in the day in July and August followed by negative residuals approaching noon show a trend that could be due to surrounding objects that may reflect or absorb more or less irradiance than is predicted by the correlation model.

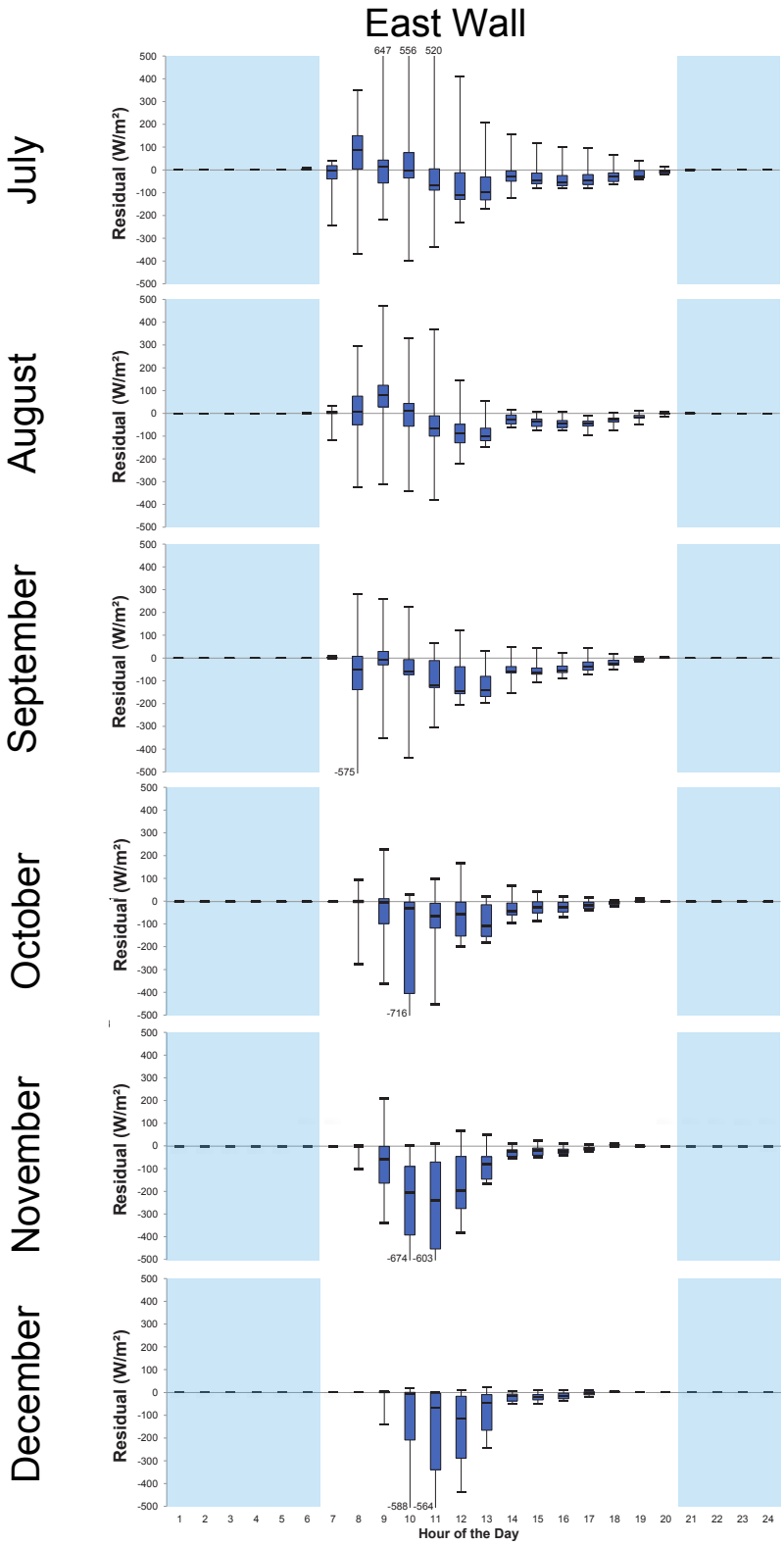


**Figure 3.5.** Monthly box and whisker plots of the residuals of hourly irradiance on the east sensor on Building 101.

Figure 3.6 shows residuals from the West sensor that are larger in the afternoon at specific times (August) and seem to shift from positive to negative at different times throughout the year without much of a trend. This is likely due to a large deciduous tree located to the West of the building that obscures the West sensor at certain times of the day in November and December as shown in Figure 3.8. Additionally, as the leaves fall off in the Autumn months and are not present in November and December, the magnitude of the residuals is decreased.

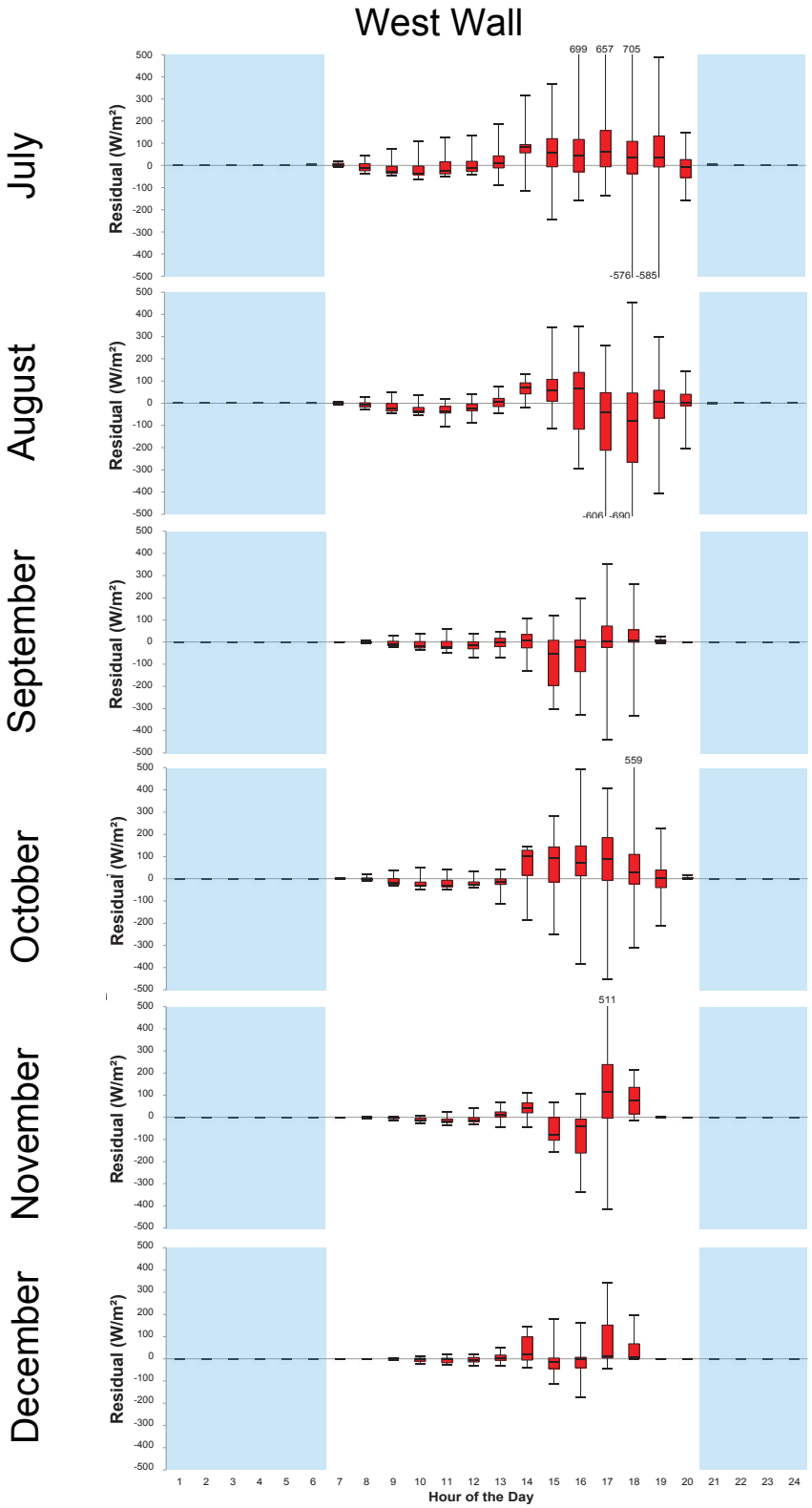


**Figure 3.6.** Monthly box and whisker plots of the residuals of hourly irradiance on the west sensor on Building 101.

Figure 3.7 shows residuals from the North sensor with a trend in July and August where the residuals are negative in the morning and positive in the afternoon. Here, there is a tree located near the Northeast corner of the building that sometimes obscures the North sensor as shown in Figure 3.8. Due to the rotation of the building of 6 degrees West of North, in July and August the correlation model anticipates the sensor to see some beam irradiation in the morning and be shaded in the afternoon. However, because of the tree, the sensor is in shade in the morning, and sees some reflection off of the tree in the afternoon. In the later months, August through December, the residuals are negative showing that the tree is simply making it even darker on the North side than the model is anticipating.

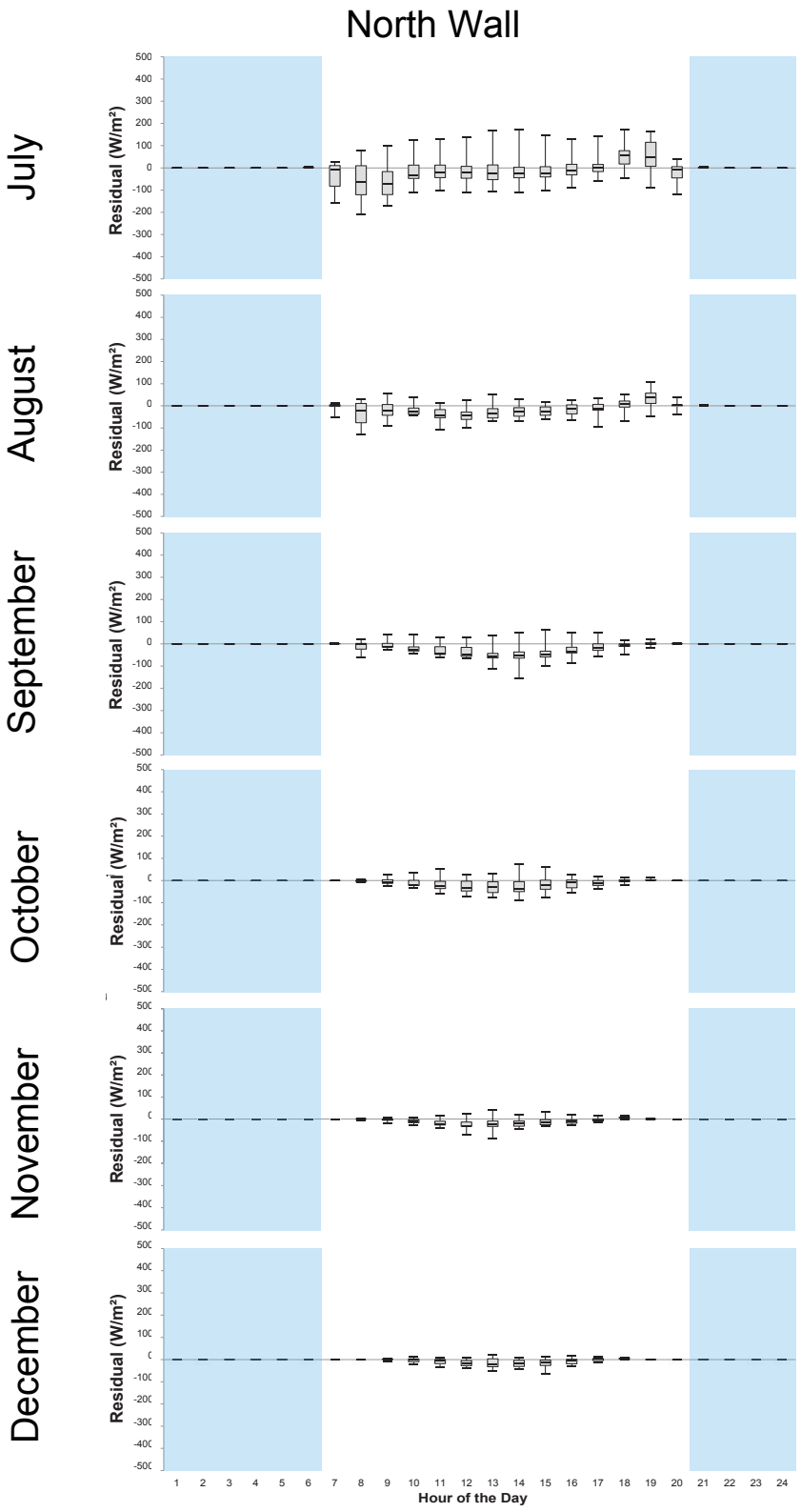


**Figure 3.7.** Monthly box and whisker plots of the residuals of hourly irradiance on the north sensor on Building 101.

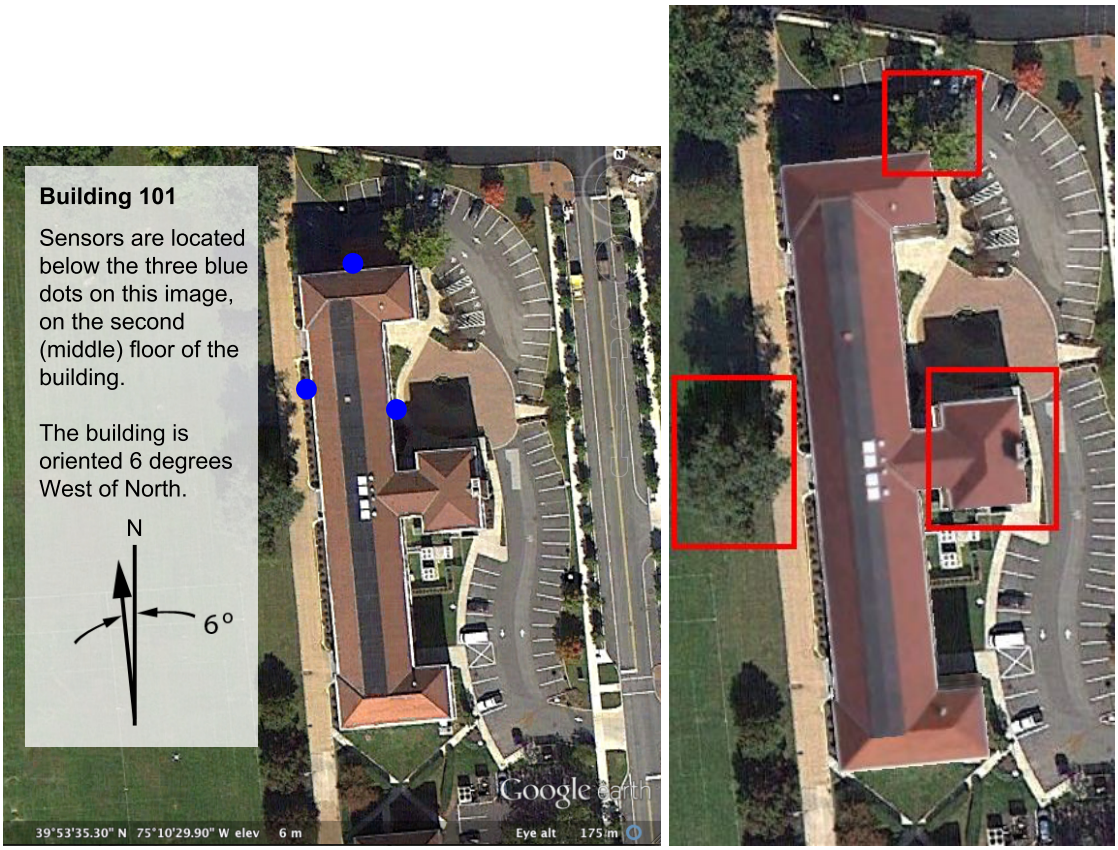


**Figure 3.8.** (Left) The pyranometers mounted on the East, West, and North walls are shown as blue dots and (right) potential shading objects are highlighted in red.

To determine whether or not the residuals between the modeled and measured data is statistically significant, Welch's $t$-test was employed. After employing Equations 2.4, 2.5, and 2.7, the $t$-statistic was calculated for each wall (East, West, and North) during each month of the year. The $t$-statistic values are shown in Figure 3.9. The positive $t$-statistic values imply larger averages for the modeled data versus the measured data while the negative values imply larger averages for the measured data versus the modeled data. However, when comparing the $t$-statistic values in Figure A.1, the absolute values of the $t$-statistics are used. As a result, there is no significance to the positive and negative values for this particular study.

| t-statistic | | | | | | |
|---|---|---|---|---|---|---|
| Wall | July | August | September | October | November | December |
| East | 0.71 | 2.01 | 2.35 | 3.41 | 7.66 | 6.70 |
| West | -2.05 | -0.17 | -0.91 | 1.27 | -0.31 | -1.40 |
| North | 1.13 | 2.90 | 4.72 | 3.24 | 2.64 | 2.30 |

**Figure 3.9.** $t$-statistic values for the irradiance on the East, West, and North walls between the months of July and December.

In addition to calculating the $t$-statistic for each wall of each month, the degrees of freedom were also calculated. The degrees of freedom are necessary for the comparison of the $t$-statistics in the probability table. Employing Equation 2.6, the degrees of freedom were calculated for each wall of each month as shown in Figure 3.10. Due to the similarity in the critical values of the $t$ distribution in the probability table when the degree of freedom values are so high ($> 700$), the degree of freedom values as shown in Figure 3.10 were rounded down to their nearest value in the table. As a result, the degrees of freedom considered were $\nu = 700$ and $\nu = 1000$. Looking at a confidence interval of 95%, the critical $t$ values are 1.963 and 1.962 for $\nu = 700$ and $\nu = 1000$, respectively.

| Degrees of Freedom | | | | | | |
|---|---|---|---|---|---|---|
| **Wall** | **July** | **August** | **September** | **October** | **November** | **December** |
| East | 1479 | 1085 | 1355 | 1079 | 736 | 749 |
| West | 1417 | 1086 | 1305 | 1441 | 1421 | 1341 |
| North | 1401 | 1062 | 1053 | 1175 | 1252 | 1242 |

**Figure 3.10.** Degree of freedom values for the irradiance on the East, West, and North walls between the months of July and December.

Comparing the $t$-statistics shown in Figure 3.9 with the critical $t$ values shown in Figure 3.10 yielded results concerning the statistical significance of the irradiance values between the modeled and measured data. For $t$-statistics greater than the critical $t$ value at its corresponding degree of freedom, the null hypothesis was rejected. Instances where the null hypothesis was rejected were highlighted in red in Figure 3.11. This means that the measured irradiance values were statistically different from the modeled irradiance values. If, on the other hand, the $t$-statistics were less than the critical $t$ value at its corresponding degree of freedom, then the null hypothesis was accepted. Instances where the null hypothesis was accepted were highlighted in green in Figure 3.11. This means that the measured irradiance values were not statistically different from the modeled irradiance values. The results for the East, West, and North walls for the months of July to December are shown in Figure 3.11.

| **Wall** | **July** | **August** | **September** | **October** | **November** | **December** |
|---|---|---|---|---|---|---|
| East | | | | | | |
| West | | | | | | |
| North | | | | | | |

= Reject null hypothesis

= Accept null hypothesis

**Figure 3.11.** Results of the $t$-test showing whether or not the null hypothesis was rejected.

The results of the $t$-test are very telling when comparing the modeled and measured irradiance data. For the East and North façades, it can be said with 95% confidence that the measured irradiance values during the month of July are represented well enough by the modeled data from Avondale. Due to the high solar altitude angle, there is no concern with shading from the Southeastern wingwall on the East sensor. Also, the sun rises and sets in the Northern regions which allows the North sensor on Building 101 to more closely resemble the North modeled irradiance values in Avondale. However, between the months of August and December, the measured data cannot be represented by the modeled data from Avondale. The solar altitude angle decreases from August to December which led to less beam irradiance incident on the North façade of Building 101 but larger diffuse component values. In addition, the tree to the Northeast was providing additional shading as the sun dropped lower in the sky. As discussed earlier, the occasional and eventual complete shading on the East sensor between the months of October and December skewed the measured irradiance values and created much larger irradiance residuals during that time period.

On the other hand, the West façade of Building 101 has the opposite effect as time progresses. In July, the measured irradiance on the West wall was statistically different than the modeled data, which is most likely due to the shading provided by the tree located to the Southwest of the sensor. However, from August to December, it can be said with 95% confidence that the irradiance values for the West wall were statistically similar or the same as the modeled data. During the fall and winter months, when the Southwest tree lost all its foliage, there was very little shading as a result of the tree's location. This allowed for irradiance values to be more representative of the irradiance values from Avondale.

Chapter 4

# Conclusion

Measured irradiance on the plane of array for building surfaces offers different results than are obtained by modeled correlations from global horizontal irradiance. Trends and biases in the errors show certain objects near to the building that both increase and decrease incident irradiance depending on the time of year and the time of day. For example, the East wall experiences positive residuals during the morning but negative residuals in the afternoon in July and August which is likely due to surrounding objects either reflecting or absorbing more or less irradiance than is predicted by the Avondale correlation model. Also, the decreases in the residuals for the West wall between the months of October and December are likely a result of the deciduous tree losing its foliage. During the summer months, rather than the North sensor seeing increased beam irradiance in the morning, the nearby tree instead provides shading during the morning. The results of a $t$-test proved with 95% confidence these phenomena. Between the months of August and December for the North and East walls and during the month of July for the West wall, the measured irradiance values were statistically different from the modeled irradiance values due mostly to surrounding objects. As a result, the modeled data cannot represent the measured data during the months. Some of the more significant errors can be accounted for in future work through more accurate modeling that includes the surrounding objects (e.g. trees) and their material properties. However, without an advanced energy model accounting for accurate surroundings, residuals on the order of hundreds of watts per meter squared were observed.

Such detailed energy models are atypical, far outside of the normal commissioning, operation, and maintenance of a commercial building due to expense. Use of local sensors that report actual shading conditions upon a building are actually more useful in this case, as a shaded region will lead to reduced energy gains for entire zones of the building, and require control response to maintain a comfortable indoor environment. Solar irradiance varies significantly on a building's many surfaces based on the environment and surrounding objects. This case study shows how local *plane of array* irradiance data can be informative to a building control system.

# Appendix A

Appendix B Statistical Tables and Graphs App19

**TABLE B.3 (cont.)** Critical Values of the $t$ Distribution

| $\nu$ | $\alpha(2)$: 0.50 / $\alpha(1)$: 0.25 | 0.20 / 0.10 | 0.10 / 0.05 | 0.05 / 0.025 | 0.02 / 0.01 | 0.01 / 0.005 | 0.005 / 0.0025 | 0.002 / 0.001 | 0.001 / 0.0005 |
|---|---|---|---|---|---|---|---|---|---|
| 52 | 0.679 | 1.298 | 1.675 | 2.007 | 2.400 | 2.674 | 2.932 | 3.255 | 3.488 |
| 54 | 0.679 | 1.297 | 1.674 | 2.005 | 2.397 | 2.670 | 2.927 | 3.248 | 3.480 |
| 56 | 0.679 | 1.297 | 1.673 | 2.003 | 2.395 | 2.667 | 2.923 | 3.242 | 3.473 |
| 58 | 0.679 | 1.296 | 1.672 | 2.002 | 2.392 | 2.663 | 2.918 | 3.237 | 3.466 |
| 60 | 0.679 | 1.296 | 1.671 | 2.000 | 2.390 | 2.660 | 2.915 | 3.232 | 3.460 |
| 62 | 0.678 | 1.295 | 1.670 | 1.999 | 2.388 | 2.657 | 2.911 | 3.227 | 3.454 |
| 64 | 0.678 | 1.295 | 1.669 | 1.998 | 2.386 | 2.655 | 2.908 | 3.223 | 3.449 |
| 66 | 0.678 | 1.295 | 1.668 | 1.997 | 2.384 | 2.652 | 2.904 | 3.218 | 3.444 |
| 68 | 0.678 | 1.294 | 1.668 | 1.995 | 2.382 | 2.650 | 2.902 | 3.214 | 3.439 |
| 70 | 0.678 | 1.294 | 1.667 | 1.994 | 2.381 | 2.648 | 2.899 | 3.211 | 3.435 |
| 72 | 0.678 | 1.293 | 1.666 | 1.993 | 2.379 | 2.646 | 2.896 | 3.207 | 3.431 |
| 74 | 0.678 | 1.293 | 1.666 | 1.993 | 2.378 | 2.644 | 2.894 | 3.204 | 3.427 |
| 76 | 0.678 | 1.293 | 1.665 | 1.992 | 2.376 | 2.642 | 2.891 | 3.201 | 3.423 |
| 78 | 0.678 | 1.292 | 1.665 | 1.991 | 2.375 | 2.640 | 2.889 | 3.198 | 3.420 |
| 80 | 0.678 | 1.292 | 1.664 | 1.990 | 2.374 | 2.639 | 2.887 | 3.195 | 3.416 |
| 82 | 0.677 | 1.292 | 1.664 | 1.989 | 2.373 | 2.637 | 2.885 | 3.193 | 3.413 |
| 84 | 0.677 | 1.292 | 1.663 | 1.989 | 2.372 | 2.636 | 2.883 | 3.190 | 3.410 |
| 86 | 0.677 | 1.291 | 1.663 | 1.988 | 2.370 | 2.634 | 2.881 | 3.188 | 3.407 |
| 88 | 0.677 | 1.291 | 1.662 | 1.987 | 2.369 | 2.633 | 2.880 | 3.185 | 3.405 |
| 90 | 0.677 | 1.291 | 1.662 | 1.987 | 2.368 | 2.632 | 2.878 | 3.183 | 3.402 |
| 92 | 0.677 | 1.291 | 1.662 | 1.986 | 2.368 | 2.630 | 2.876 | 3.181 | 3.399 |
| 94 | 0.677 | 1.291 | 1.661 | 1.986 | 2.367 | 2.629 | 2.875 | 3.179 | 3.397 |
| 96 | 0.677 | 1.290 | 1.661 | 1.985 | 2.366 | 2.628 | 2.873 | 3.177 | 3.395 |
| 98 | 0.677 | 1.290 | 1.661 | 1.984 | 2.365 | 2.627 | 2.872 | 3.175 | 3.393 |
| 100 | 0.677 | 1.290 | 1.660 | 1.984 | 2.364 | 2.626 | 2.871 | 3.174 | 3.390 |
| 105 | 0.677 | 1.290 | 1.659 | 1.983 | 2.362 | 2.623 | 2.868 | 3.170 | 3.386 |
| 110 | 0.677 | 1.289 | 1.659 | 1.982 | 2.361 | 2.621 | 2.865 | 3.166 | 3.381 |
| 115 | 0.677 | 1.289 | 1.658 | 1.981 | 2.359 | 2.619 | 2.862 | 3.163 | 3.377 |
| 120 | 0.677 | 1.289 | 1.658 | 1.980 | 2.358 | 2.617 | 2.860 | 3.160 | 3.373 |
| 125 | 0.676 | 1.288 | 1.657 | 1.979 | 2.357 | 2.616 | 2.858 | 3.157 | 3.370 |
| 130 | 0.676 | 1.288 | 1.657 | 1.978 | 2.355 | 2.614 | 2.856 | 3.154 | 3.367 |
| 135 | 0.676 | 1.288 | 1.656 | 1.978 | 2.354 | 2.613 | 2.854 | 3.152 | 3.364 |
| 140 | 0.676 | 1.288 | 1.656 | 1.977 | 2.353 | 2.611 | 2.852 | 3.149 | 3.361 |
| 145 | 0.676 | 1.287 | 1.655 | 1.976 | 2.352 | 2.610 | 2.851 | 3.147 | 3.359 |
| 150 | 0.676 | 1.287 | 1.655 | 1.976 | 2.351 | 2.609 | 2.849 | 3.145 | 3.357 |
| 160 | 0.676 | 1.287 | 1.654 | 1.975 | 2.350 | 2.607 | 2.846 | 3.142 | 3.352 |
| 170 | 0.676 | 1.287 | 1.654 | 1.974 | 2.348 | 2.605 | 2.844 | 3.139 | 3.349 |
| 180 | 0.676 | 1.286 | 1.653 | 1.973 | 2.347 | 2.603 | 2.842 | 3.136 | 3.345 |
| 190 | 0.676 | 1.286 | 1.653 | 1.973 | 2.346 | 2.602 | 2.840 | 3.134 | 3.342 |
| 200 | 0.676 | 1.286 | 1.653 | 1.972 | 2.345 | 2.601 | 2.839 | 3.131 | 3.340 |
| 250 | 0.675 | 1.285 | 1.651 | 1.969 | 2.341 | 2.596 | 2.832 | 3.123 | 3.330 |
| 300 | 0.675 | 1.284 | 1.650 | 1.968 | 2.339 | 2.592 | 2.828 | 3.118 | 3.323 |
| 350 | 0.675 | 1.284 | 1.649 | 1.967 | 2.337 | 2.590 | 2.825 | 3.114 | 3.319 |
| 400 | 0.675 | 1.284 | 1.649 | 1.966 | 2.336 | 2.588 | 2.823 | 3.111 | 3.315 |
| 450 | 0.675 | 1.283 | 1.648 | 1.965 | 2.335 | 2.587 | 2.821 | 3.108 | 3.312 |
| 500 | 0.675 | 1.283 | 1.648 | 1.965 | 2.334 | 2.586 | 2.820 | 3.107 | 3.310 |
| 600 | 0.675 | 1.283 | 1.647 | 1.964 | 2.333 | 2.584 | 2.817 | 3.104 | 3.307 |
| 700 | 0.675 | 1.283 | 1.647 | 1.963 | 2.332 | 2.583 | 2.816 | 3.102 | 3.304 |
| 800 | 0.675 | 1.283 | 1.647 | 1.963 | 2.331 | 2.582 | 2.815 | 3.100 | 3.303 |
| 900 | 0.675 | 1.282 | 1.647 | 1.963 | 2.330 | 2.581 | 2.814 | 3.099 | 3.301 |
| 1000 | 0.675 | 1.282 | 1.646 | 1.962 | 2.330 | 2.581 | 2.813 | 3.098 | 3.300 |
| $\infty$ | 0.6745 | 1.2816 | 1.6449 | 1.9600 | 2.3263 | 2.5758 | 2.8070 | 3.0902 | 3.2905 |

If a critical value is needed for degrees of freedom not on this table, one may conservatively employ the next smaller $\nu$ that is on the table. Or, the needed critical value, for $\nu < 1000$, may be calculated by linear interpolation, with an error of no more than 0.001. If a little more accuracy is desired, or if the needed $\nu$ is $> 1000$, then harmonic interpolation should be used.

Critical values of $t$ for infinity degrees of freedom are related to critical values of Z and $\chi^2$ as

$$t_{\alpha(1),\infty} = Z_{\alpha(1)} \quad \text{and} \quad t_{\alpha(1),\infty} = Z_{\alpha(2)} = \sqrt{\chi^2_{\alpha,1}}.$$

**Figure A.1.** Probability table used to compare the $t$-statistics to the critical $t$ values to determine the statistical significance between the modeled and measured irradiance values.[3]

# Bibliography


[1] "Kipp & Zonen Silicon Pyranometer SP Lite," Microsoft Word.

[2] (2012), "Ground Reflectance," .
URL `http://www.bembook.ibpsa.us/index.php?title=Ground_Reflectance`

[3] Zar, J. H. (1996) *Biostatistical Analysis*, third ed., Prentice Hall.

[4] EIA (2011), "Energy Consumption by Sector," .
URL `http://www.eia.gov/totalenergy/data/annual/pdf/sec2.pdf`

[5] Kalogirou, S. A. (2009) *Solar Energy Engineering: Processes and Systems*, Elsevier.

[6] Hub, E. (2012), "About EEB Hub," .
URL `http://eebhub.org/about-eebhub`

[7] ——— (2012), "Navy Yard Building 101," .
URL `http://www.eebhub.org/projects-list/navy-yard-building-101/`

[8] (2012), Website.
URL `http://cloud.cdhenergy.com/bldg101/`

[9] NOAA, "About NCDC," .
URL `http://www.ncdc.noaa.gov/about-ncdc`

[10] ———, "Measured Elements," .
URL `http://www.ncdc.noaa.gov/crn/elements.html`

[11] Gueymard, C. A. (2009) "Direct and indirect uncertainties in the prediction of tilted irradiance for solar engineering applications," *Solar Energy*, **83**, pp. 432–444.

[12] Duffie, J. A. and W. A. Beckman (2006) *Solar Engineering of Thermal Processes*, 3rd ed., John Wiley and Sons, Inc.

[13] Dupont, R., J. Siemer, and M. Hirsch (2010) "How Much Sunlight?" *PHOTON*, **12**, pp. 50–67.

[14] Hay, J. E. (1979) "Calculation of monthly mean solar radiation for horizontal and inclined surfaces," *Solar Energy*, **23**, pp. 301–307.

[15] Maxwell, E., T. Stoffel, and R. Bird (1986) *Measuring and Modeling Solar Irradiance on Vertical Surfaces*, *Tech. rep.*, Solar Energy Research Institute.

[16] Stoffel, T. L., E. L. Maxwell, R. E. Bird, and D. R. Myers (1987) "Solar Irradiance on Vertical Surfaces," *Passive Solar Journal*, **4**, pp. 187–210.

[17] Perez, R., P. Ineichen, R. Seals, J. Michalsky, and R. Stewart (1990) "Modeling daylight availability and irradiance components from direct and global irradiance," *Solar Energy*, **44**, pp. 271–289.

[18] Reindl, D., W. Beckman, and J. Duffie (1990) "Evaluation of hourly tilted surface radiation models," *Solar Energy*, **45**, pp. 9–17.

[19] Psiloglou, B. and H. Kambezidis (2009) "Estimation of the ground albedo for the Athens area, Greece," *Journal of Atmospheric and Solar-Terrestrial Physics*, **71**, pp. 943–954.

[20] Li, H., J. Harvey, and A. Kendall (2013) "Field measurement of albedo for different land cover materials and effects on thermal performance," *Building and Environment*, **59**, pp. 536–546.

[21] (2012), Website.
URL `http://www.ncdc.noaa.gov/crn/report`

[22] Welch, B. (1947) "The Generalization of "Student's" Problem When Several Different Population Variances Are Involved," *Biometrika*, **34**(1-2), pp. 28–35.

# Academic Vita

**SCOTT BURGER**

scottburger1090@gmail.com

## Education

B.S., Energy Engineering, 2013, Penn State University, University Park, PA

## Honors and Awards

- Schreyer Academic Excellence Scholarship, The Schreyer Honors College, 2009-2013
- General Scholarship in Energy and Mineral Engineering, College of Earth and Mineral Sciences, 2012-2013

## Association Memberships

- American Solar Energy Society
- National Society of Collegiate Scholars

## Professional Experience

Sun Directed
Bellefonte, Pennsylvania
*Solar Installer*
June 2012-August 2012

- Assisted in the installations of a 11.5 kW ground-mounted photovoltaic system and a roof-mounted solar hot water system
- Helped to replace malfunctioning microinverters on a roof-mounted photovoltaic system

PECO Energy Company
Berwyn, Pennsylvania
*Overhead Transmission Intern*
May 2011-August 2011

- Demonstrated organizational skills through managing 200 overhead transmission lines using Microsoft Excel and Excel Visual Basic macros
- Participated in teamwork meetings to review daily safety lessons and daily job reports
- Received field experience for mobile transformer installation and high voltage transmission grounding

**Research Experience**

Penn State University
University Park, Pennsylvania
*Undergraduate Researcher*
May 2012-May 2013

- Used Microsoft Excel VBA to organize data pertaining to solar radiation collected from pyranometers mounted on Philadelphia Navy Yard buildings
- Performed data simulations of Philadelphia Navy Yard buildings using Transient System Simulation Tool
- Modeled and mapped the Philadelphia Navy Yard using Esri's ArcGIS software
- Performed inverse modeling to accurately estimate global horizontal irradiation from data collected from plane of array pyranometers

**Research Interests**

I have broad interests in renewable energy, particularly the integration of solar energy with buildings. Specifically, I am interested in the effect of solar insolation on building energy control systems and how to design smarter energy control systems.

**Professional Presentations**

Irradiance Modeling Variance on Vertical Plane of Array Surfaces, The American Solar Energy Society Conference, Baltimore Convention Center, April 16-20

**Publications and Papers**

Burger, S. (2013). Irradiance Modeling Variance on Vertical Plane of Array Surfaces. University Park, PA, The Pennsylvania State University: 1-7.